Bioorganic & Medicinal Chemistry 16 (2008) 8635–8642

Contents lists available at ScienceDirect

Bioorganic & Medicinal Chemistry

journal homepage: www.elsevier.com/locate/bmc

Molecular modeling studies toward the structural optimization of new cyclopeptide-based HDAC inhibitors modeled on the natural product FR235222

Simone Di Micco [a], Stefania Terracciano [a], Ines Bruno [a], Manuela Rodriquez [a], Raffaele Riccio [a], Maurizio Taddei [b], Giuseppe Bifulco [a,*]

[a] Dipartimento di Scienze Farmaceutiche, Università degli Studi di Salerno, Via Ponte don Melillo, 84084 Fisciano, Salerno, Italy
[b] Dipartimento Farmaco Chimico Tecnologico, Università di Siena Via A. Moro 2, 53100 Siena, Italy

ARTICLE INFO

Article history:
Received 26 May 2008
Revised 28 July 2008
Accepted 1 August 2008
Available online 6 August 2008

Keywords:
Histone deacetylase inhibitors
Molecular docking
2D NMR
DFT

ABSTRACT

The natural cyclopeptide FR235222 is a potent HDAC inhibitor displaying relevant multiple anticancer effects and is considered an attractive lead compound for the generation of new and more effective antitumor therapeutics. Recently, we have synthesized a small collection of FR235222 simplified analogues which showed interesting biological activities. These results encouraged us to further explore the structural determinants responsible for the activity of this class of HDAC inhibitors in order to gain guidelines for the rational design of new derivatives with putative higher affinity for this target. In the present paper, we report the results obtained, docking these ligands in the binding pocket of HDLP, an HDAC homologue.

1. Introduction

Modification of histone acetylation level, promoted by HAT and HDAC enzymes, has been recognized to play an important role in the epigenetic modulation of gene expression; in fact this well-known post-translational mechanism is highly involved in the modulation of chromatin plasticity and in the regulation of transcriptional factors accessibility to DNA[1]; therefore the disruption of histone acetylation pattern is supposed to determine transcriptional disorders and is related to several malignant diseases.[2] Inhibition of HDAC enzyme has proven to induce antiproliferative effects and to promote cellular differentiation. For these reasons, the discovery of new agents targeting HDAC enzyme is considered of great interest for the development of anticancer drugs.[3] As part of our efforts to investigate new synthetic targets useful for the discovery of novel anticancer therapeutics, we focused our attention on the natural product FR235222[4] (Scheme 1), a potent cyclopeptide inhibitor of HDAC.[5]

We used this metabolite as lead compound to design new cyclopeptide structures, taking into account the FR235222 binding mode with the active site of HDAC.[5a] Recently, we performed the synthesis of a small collection of FR235222 analogues (**1**–**10**, Scheme 2) with the aim to simplify some crucial synthetic features connected with the natural product as well as to explore the effects on the activity of some punctual aminoacidic substitutions of the tetrapeptidic core.[6]

The analogues **1**–**5** conserved the absolute configuration of natural progenitor to the C9 (Scheme 1), whereas **6**–**10** presented an inverted configuration to the same carbon. The α hydroxy-ketone function was fundamental to inhibit the enzyme, because it coordinated the zinc ion that was the prosthetic group of the HDAC. Thus, we synthesized analogues **6**–**10** with an inverted configuration to analyze the influence on biological enzymatic inhibition.

On the basis of the biological behavior of these products,[6] we realized that it is possible to modulate the potency of these ligands by increasing the lipophilicity of some AA residues within the cycle and by leaving unchanged the Ahoda residue representing the Zn chelating element. These findings confirmed us that the cyclopeptide cap group is highly involved in selective hydrophobic binding interactions at the rim of the catalytic pocket, and is able to project the Zn chelating element at an optimal distance in the tube-like cavity, to interact with prosthetic group.

Compounds **1**, **2**, and **3** showed a better pharmacological profile compared to the parent compound, for these reasons we decided to gain new detailed molecular insights into their inhibitory action, taking advantage from docking calculations. In a recent study, on other bioactive tetrapeptide ligands, we also invested many efforts to refine more accurately factors affecting the calculated binding energy value reaching a good qualitative accordance between theoretical K_D and biological essays results.[7] In particular, we refined some enzyme calculation parameters related to the electrostatic

* Corresponding author. Tel.: +39 089969741; fax: +39 089969602.
E-mail address: bifulco@unisa.it (G. Bifulco).

0968-0896/$ - see front matter © 2008 Elsevier Ltd. All rights reserved.
doi:10.1016/j.bmc.2008.08.003

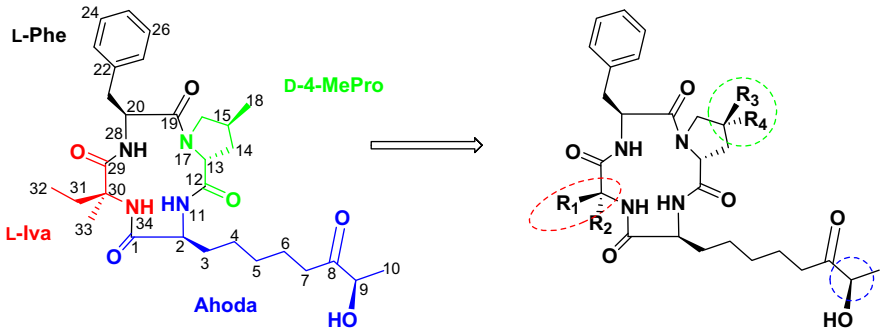

Scheme 1. Molecular structure of FR235222. The skeleton used for the synthesis of **1**–**10,** is also sketched highlighting the points of synthetic modifications.

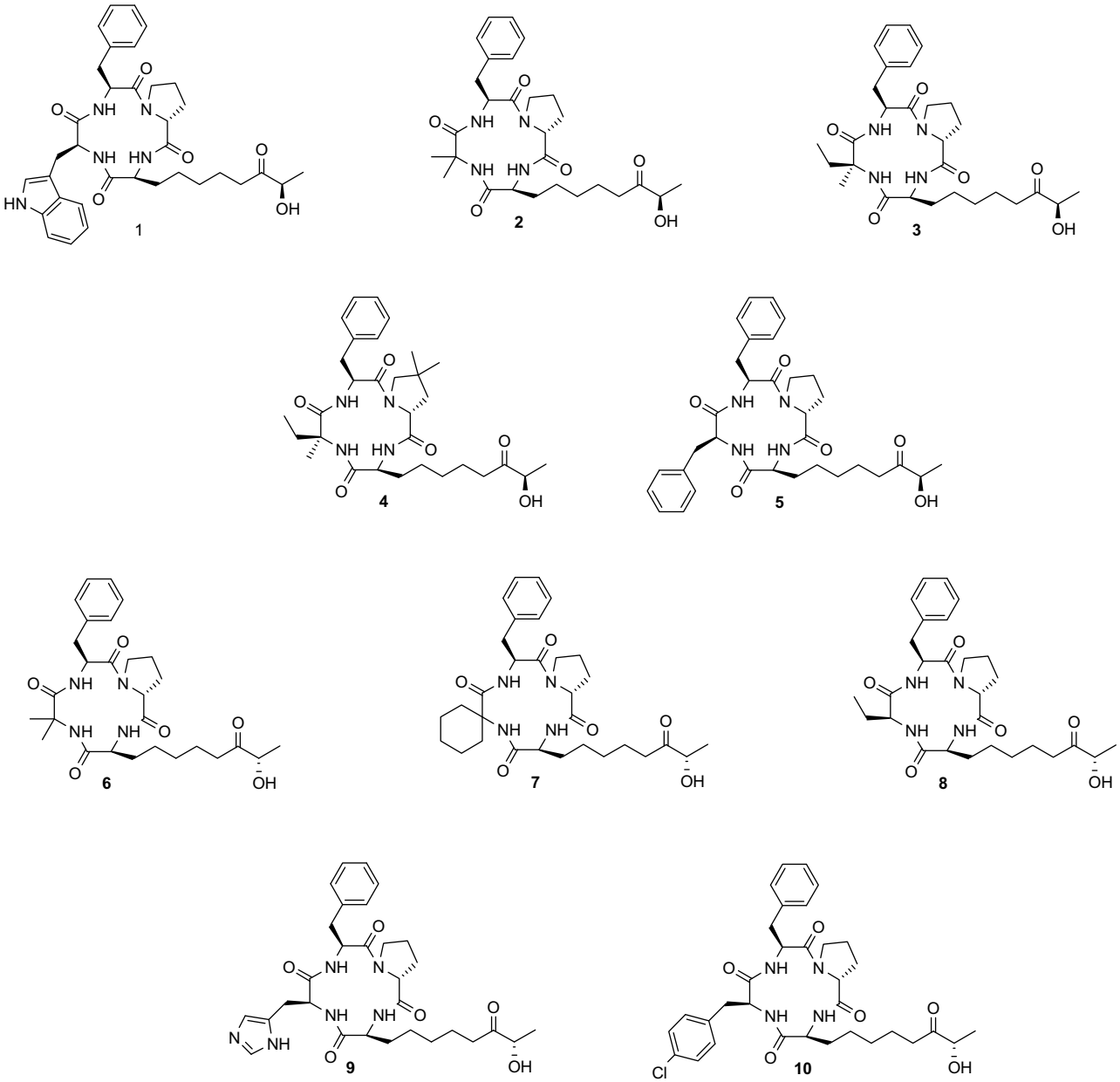

Scheme 2. Molecular structures of compounds **1**–**10**.

and van der Waals terms of binding energy. About the electrostatic contribution, we calculated the charges of HDLP[8] active site at quantum mechanical (QM) level and used for van der Waals term the well depth and zinc radius proposed by Stote and Karplus. [9] In the present study, we utilized our defined protein model, encouraged by good results obtained in our previous work.[7]

Moreover, the fully elucidated solution structures of our products were obtained by 2D NMR spectroscopy, then, on the basis of QM approach their energies and conformations were optimized and were used in the docking studies as starting conformations. On so QM refined geometries, we also calculated the point charges at DFT/B3LYP level and used for docking calculations.

2. Results and discussion

2.1. Solution structure determination

The DMSO solution-state structures were obtained by 2D NMR spectroscopy and were used as the initial conformations in the docking study (see next section).

The NMR spectra of all compounds showed a double pattern of resonances due to *cis–trans* conformational equilibrium of peptide bond formed by amine and carboxylic groups of proline and phenylalanine residues, respectively (Scheme 3).

We have performed a complete assignment of the ^{1}H and ^{13}C resonances of both isomers by the analysis of homo and heteronuclear 2D NMR experiments (for the chemical shifts values, see Table S1–S10). In particular $^{1}H–^{13}C$ HSQC and $^{1}H–^{13}C$ HMBC NMR sequences were helpful to group the double networks of resonances very similar between them. Successively, the two isomers were distinguished by searching for typical dipolar couplings observed in 2D-ROESY NMR experiments.[10] In detail, the *trans-isomers were* characterized by dipolar couplings between H_α of phenylalanine and H_δ of proline (Fig 1a), whereas the *cis-isomer* showed ROEs contacts between H_α of proline and H_β of phenylalanine (Fig. 1b).

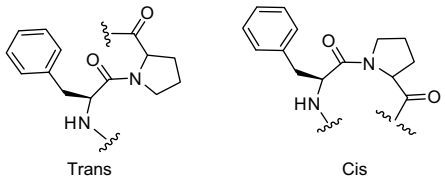

Scheme 3. *trans* and *cis* conformations of peptide bond between amine and carboxylic groups of proline and phenylalanine residues, respectively.

For each *cis-* and *trans-isomers* of **1**–**7** and **10** structures, a set of distance restraints (see Supporting information, Table S11–S18) were collected from 2D-ROESY NMR experiments (t_{mix} = 100 ms) and used in the molecular dynamics calculations (500 K). Details for setting upper and lower bound distances for the ROE constraints are given in Section 5. Thus, we obtained the solution structures for both *cis-* and *trans-isomers* of **1**–**7** and **10**.

The NMR structure backbone analysis of **1**–**7** and **10** *cis*/*trans*-isomers did not reveal the presence of any identifiable turns or defined secondary structure, and allowed to trace the differences among all the analogues with regard to their peptide bond spatial arrangements. For what concerns the *cis* conformation (Fig. 2) of compound **1**, the amide NHs of Ahoda and Trp residues point above the plane delimited by the peptide backbone and in the opposite direction with respect to the NH of phenylalanine. On the other hand, in the *cis-isomers* of **2**, **3**, **4**, and **6**, the NHs groups of Phe and Ahoda residues are above the cyclopeptide plane, while the position of the remaining NH functions is inverted compared to **1**.

It is noteworthy that diastereoisomers **2** and **6**, only differing for the C9 configuration, present high superposition of the 3D structures (Fig. 2). Compound **5** differs from two preceding spatial arrangements described, projecting all amide NHs above the plane delimited by peptide backbone. Structure **7** keeps a similar amide bond spatial arrangement of Ahoda residue found for **1**–**6**, and positioned down the NHs of Phe and Acc residues, with respect to the macrocycle. Analogue **10**, different from the above-described cis conformations, is characterized by a parallel alignment of the Ahoda NH group with the same function of Phe residue.

The analysis of the solution structure of the *trans-isomers* (Fig 2) revealed that in **1** the NHs of Trp and Ahoda residues are projected upon the peptide ring and in opposite direction with respect to the NH of Phe. Different from **1**, compounds **2**, **3**, **4**, and **6** conserved the topological peculiarity of the cyclopeptide bonds found for the *cis-isomers*. It is noteworthy that the *trans-epimers* **2** and **6** present the same 3D arrangement, as already found for the *cis* conformations.

Analogue **5**, compared to **1**, shows inverted arrangement of the NHs of Ahoda and Phe (bound to Pro), while **7** and **10** differ from the solution structures above described, as the NH groups point toward the same side of the macrolactame moiety.

We investigated compounds **8** and **9** through molecular dynamics calculations without experimental restraints. The full exploration of their conformational space suggested that the

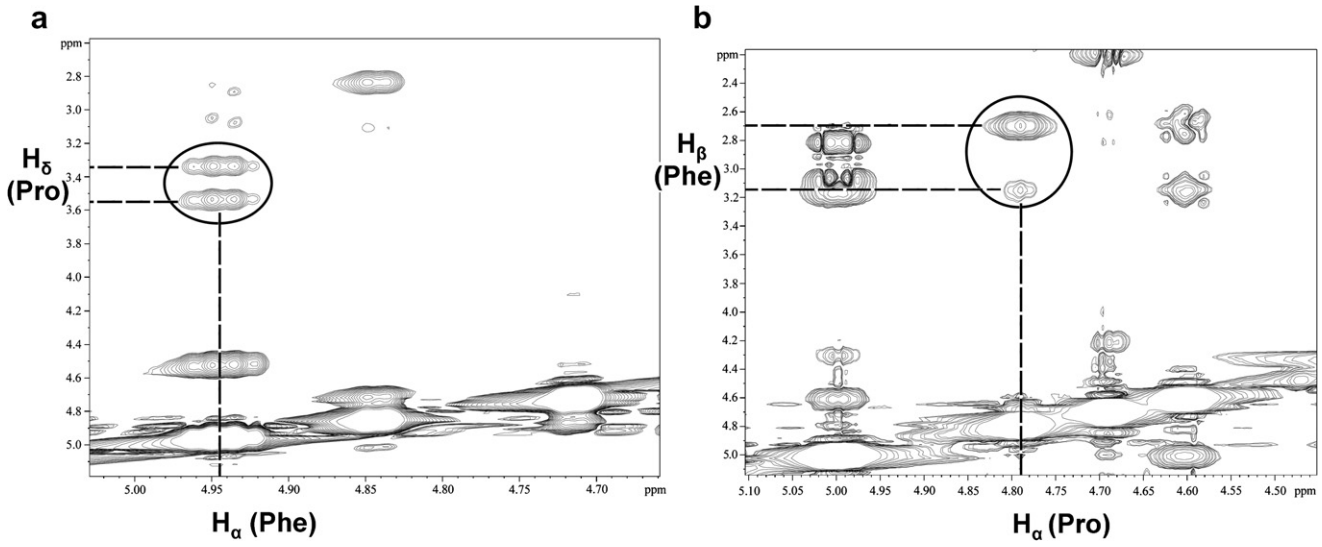

Figure 1. Expanded spectral regions of ROESY spectrum (600 MHz, 300 K, t_{mix} = 100 ms) of **6**. In (a and b) are circled typical dipolar couplings of *trans-* and *cis*-isomers, respectively.

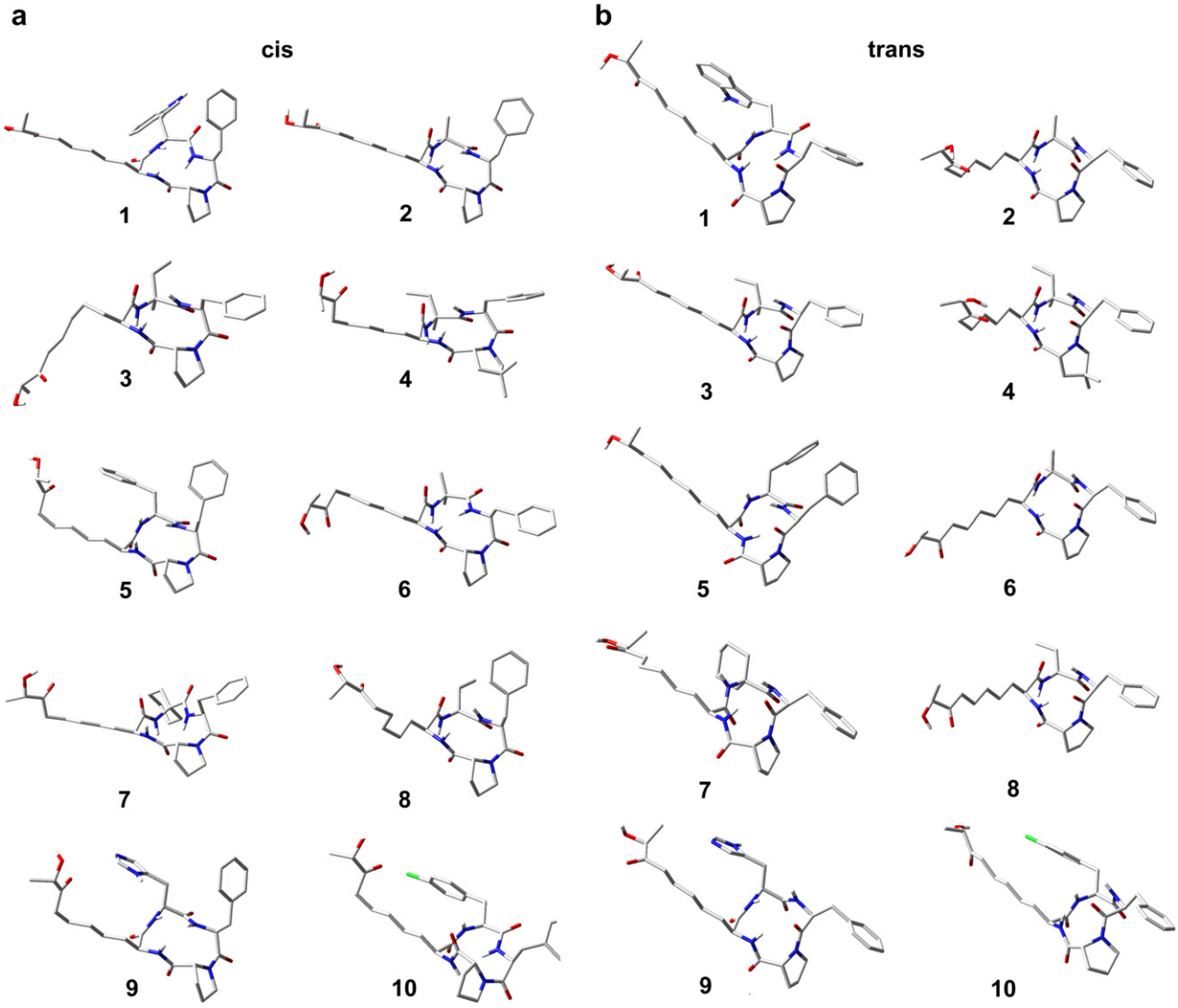

Figure 2. NMR solution-state conformations for *cis* (a) and *trans* (b) isomers of **1**–**7** and **10** obtained by restrained MD calculations, using ROESY (t_{mix} = 100 ms, 300 K) data collected at 600 MHz in DMSO-d_6. The representative conformations of **8** and **9**, found by MD calculations without experimental distances, are also shown.

cis- and *trans-isomers* of compound **8** are comparable to the minimum energy conformers of **2**, **3**, **4**, and **6** (Fig. 2). Finally, the *cis-conformer* of **9** presents the same arrangements of the cyclopeptide bonds of **5**, whereas the *trans-isomer* shows the NHs group arrangement as in **7** and **10** (Fig. 2).

3. Docking studies

As there was no 3D structure of HDAC1 available, in the docking calculations we used the homologous protein HDLP as target model.[8] Docking studies were performed on the *cis*- and *trans-isomers* of **1**–**10**, with the HDLP[8] binding pocket, using AutoDock 3.0.5 software,[11] which has been successfully used in the interpretation of the inhibitory activity of several HDAC ligands.[7,12] We analyzed the *cis*- and *trans-isomers* of **1**–**10** to evaluate if one or both isomers could be interacting with the biological target.

The partial charges of *cis*- and *trans-isomers* of ligands were calculated at DFT/B3LYP level and 6-31+G(d) basis set using the ChelpG[13] method for population analysis, and were used in the subsequent docking calculations. As described in an our previous paper,[7] the partial charges for the zinc ion and for the amino acids belonging to the catalytic center (A169, H170, D168, D258) were also obtained using the above-described procedures. For sake of simplicity, we will describe in this section only the detailed docking results for both isomers of compound **1**, as it showed the most interesting biological activity.

The analysis of *cis-conformer* revealed that the α-hydroxyl ketone is of primary importance for its interactions with catalytic site: it coordinates the zinc ion in a monodentate fashion by its carbonylic oxygen and establishes a hydrogen bond with $H^{\varepsilon 2}$ of H131 through the same oxygen. The hydroxyl group forms two hydrogen bonds, one with the carboxylate function of D168 and one with the side chain of H131.

Moreover, the C2 eight carbon aliphatic chain establishes appropriate hydrophobic contacts with the zinc-containing tubular pocket.

The macrolactam portion is accommodated in a shallow groove, formed by residues H170, F198, L265, and F141 (Fig. 3). It establishes van der Waals interactions and hydrogen bonds with H170 and F198 by the peptide carboxylic oxygen belonging to the Ahoda residue. The tetrapeptide core extends its hydrophobic contacts, thanks to the side chains of Phe, Pro, and Trp residues. In detail, the proline moiety is placed in a small hydrophobic cavity delimited by Y91, E92, and G140, whereas the phenylalanine residue

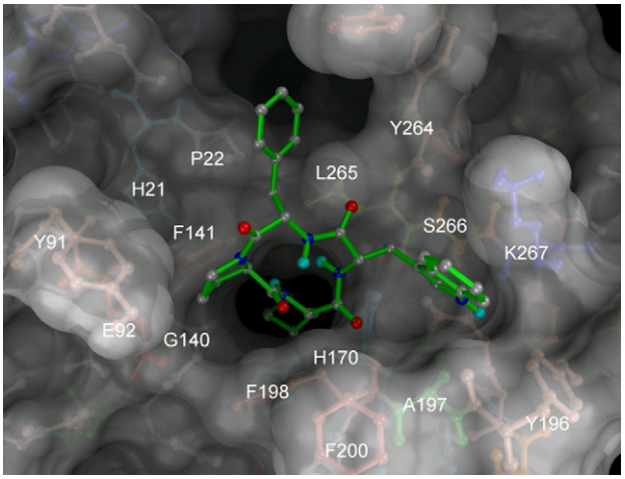

Figure 3. 3D model of the interaction between **1** (*cis*) and the HDLP binding site. The protein is represented by molecular surface, and sticks and balls. **1** is depicted by sticks (green) and balls (by atom type: C, gray; polar H, sky blue; N, dark blue; O, red). The figure highlights essential interactions: the side chains of phenylalanine, proline, and tryptophan are located in a hydrophobic pocket and the tetrapeptide core interacts with a shallow cavity on the protein surface. The Ahoda side chain establishes interactions with the 11 Å hydrophobic channel, with the zinc ion contained at the bottom and with amino acids of catalytic site.

interacts with a bigger enzymatic counterpart formed by N20, P22, Y264, L265, and F338. The tryptophan side chain is accommodated in a deep pocket delimited by the Q192, Y186, A197, F200, and K267 residues, enveloping the indole ring and strongly increasing the stability of the complex. Moreover, the NH group of the indole forms a hydrogen bond with the oxygen in the side chain of Q192.

Our docking studies on *trans-isomer* indicated that tetrapeptide core and Ahoda side chain of both docked isomers fill equivalent spaces, and the proline and tryptophan residues invert their positions (Fig. 4). In detail, the tryptophan side chain has hydrophobic interactions with residues N20, H221, P22, Y91, and F141 (Fig. 5).

The proline ring occupies the same hydrophobic cavity of tryptophan side chain observed in the *cis-isomer,* but exerting weaker contacts. In this case, the Phe side chain points outside the protein.

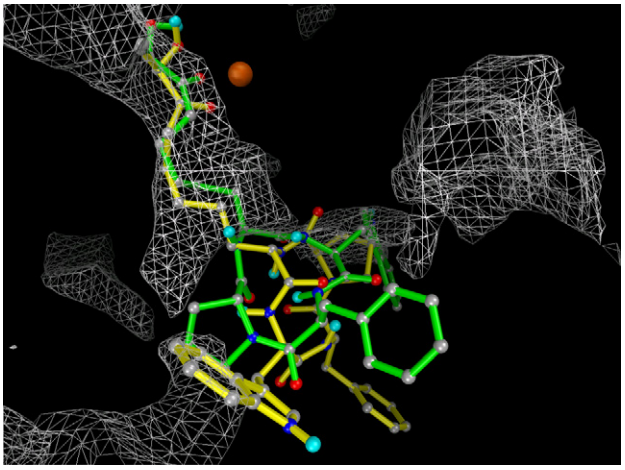

Figure 4. *cis* and *trans* of **1** superimposition in the zinc-binding site. The white mesh represents the hydrophobic pocket of the protein. The Zn^{2+} is represented by a CPK sphere in dark orange. *trans* is depicted by sticks (yellow) and balls (by atom type: C, gray; polar H, sky blue; N, blue; O, red); *cis* is shown by sticks (green) and balls (by atom type: C, gray; polar H, sky blue; N, blue; O, red). The figure highlights the similar interactions with the 11 Å deep hydrophobic channel of the Ahoda side chains, whereas the indole and proline groups of *cis* and *trans* are located on opposite sides of the protein surface hydrophobic pocket.

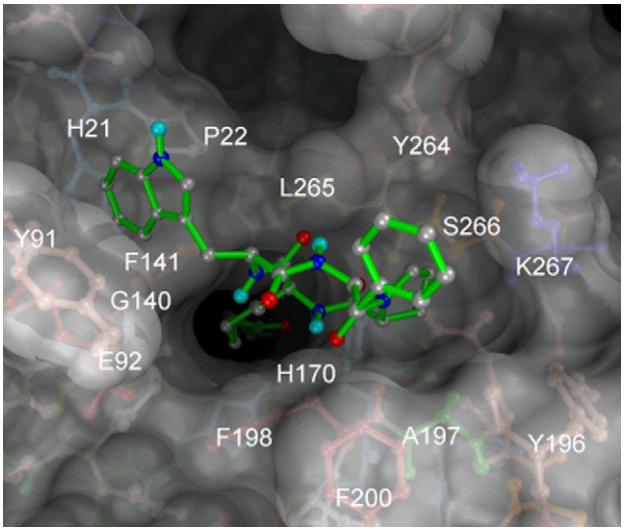

Figure 5. 3D model of the interaction between **1** (*trans*) and the HDLP binding site. The protein is represented by molecular surface, and sticks and balls. **1** is depicted by sticks (green) and balls (by atom type: C, gray; polar H, sky blue; N, dark blue; O, red). The figure highlights essential interactions: the side chains of proline and tryptophan are located in a hydrophobic pocket, and the tetrapeptide core interacts with a shallow cavity on the protein surface. The Ahoda side chain establishes interactions with the 11 Å hydrophobic channel, with the zinc ion contained at the bottom and with amino acids of catalytic site.

Moreover, the Ahoda side chain encounters the same set of interactions found for the *cis-isomer* with the tubular hydrophobic pocket. The α-hydroxyl ketone group forms a hydrogen bond with $H^{\varepsilon 2}$ of H131 and coordinated the zinc ion in a bidentate fashion. The macrolactam establishes van der Waals interactions with F141, H170, P198, and L265 amino acids.

The different arrangement of the *trans-isomer,* the suboptimal hydrophobic interactions, and the lack of some hydrogen bonds were responsible for a predicted decrease in the binding affinity to the target of about eightfold (K_i of *cis* 9.87×10^{-10} vs K_i of *trans -isomer* 7.77×10^{-9}).

Our docking studies revealed that, for **2**–**4**, *cis-* and *trans-isomers* show a comparable target affinity, giving a similar contribution to inhibit the enzymatic activity. Moreover, **2**–**4** established less hydrophobic interaction compared to **1**, because they have small alkyl substituents in place of an indole ring (see Supporting information), justifying a lower calculated K_i. Different results were obtained for compound **5**, where only one of the two isomers shows a predictable affinity expecting a lower biological activity than preceding analogues. In contrast with a single and defined family of conformations representing the efficient binding mode for **1**–**3**, *trans -isomer* of **5** shows three different conformation families, accounting for three independent, low affinity, binding modes. We established a bioactive conformation for the *cis -isomer* (see Supporting information). Also in this case there were two with aromatic side-chained amino acids, but the predicted K_i results were lower than the value calculated for **1**, although the predicted bioactive conformations of **1** and **5** were very similar between them. The two phenyl rings of **5** occupied the same hydrophobic cavities of aromatic rings observed for **1**, revealing the bulky non-polar groups as proper substituents interacting with these receptor hydrophobic counterparts. The lower calculated K_i of **5** was due to the loss of effective interactions by peptide backbone and of proline ring. Moreover, the indole moiety is bigger than a phenyl ring, and it establishes, together with a significant hydrogen bond, more efficient hydrophobic interactions with the target counterparts. The docking outcomes were confirmed by biological essays,[6] showing a good qualitative agreement between calculated and experimental data (Table 1).

Table 1
The IC_{50} (nM, inhibition of histone H4 peptide deacetylation) values of inhibition constant[a] associated with the calculated complex between **1** and **10** and HDLP

Compound	IC_{50} (nM)	K_i (*cis*)	K_i (*trans*)
FR235222	60	—	2.39×10^{-8}
1	20	9.87×10^{-10}	7.77×10^{-9}
2	30	1.64×10^{-8}	1.06×10^{-8}
3	50	1.86×10^{-8}	1.27×10^{-8}
4[c]	90	6.04×10^{-8}	4.58×10^{-8}
5[c]	280	3.69×10^{-8}	3.57×10^{-8}[d]; 8.21×10^{-8}; 2.8×10^{-7}
6	330	2.78×10^{-8}[d]; 2.81×10^{-8}[d]; 1.94×10^{-7}	1.18×10^{-8}[d]; 2.60×10^{-8}[d]; 5.28×10^{-8}
7	670	3.93×10^{-9}[d]; 1.83×10^{-8}[d]; 2.54×10^{-8}	3.91×10^{-9}[d]; 6.74×10^{-9}[d]; 6.785×10^{-9}
8	1000	9.80×10^{-9}[d]; 9.23×10^{-8}[d]; 1.10×10^{-7}	1.51×10^{-8}[d]; 5.36×10^{-8}; 5.41×10^{-8}
9	~350 000	4.74×10^{-8}[d]; 9.23×10^{-8}; 3.42×10^{-8}	6.99×10^{-9}[d]; 2.00×10^{-8}; 6.17×10^{-8}
10	ND[b]	5.45×10^{-8}[d]; 8.71×10^{-8}; 1.02×10^{-7}	6.10×10^{-9}[d]; 1.23×10^{-8}[d]; 2.34×10^{-8}

[a] The inhibition constant is expressed as M and it is measured at 293.15 K.
[b] Not determined.
[c] Inhibition constants associated to three independent, low affinity, binding modes (see text).
[d] Compounds **6**–**10** inhibition constants values for complexes showing the Ahoda side chain outside the 11 Å deep hydrophobic channel (see text).

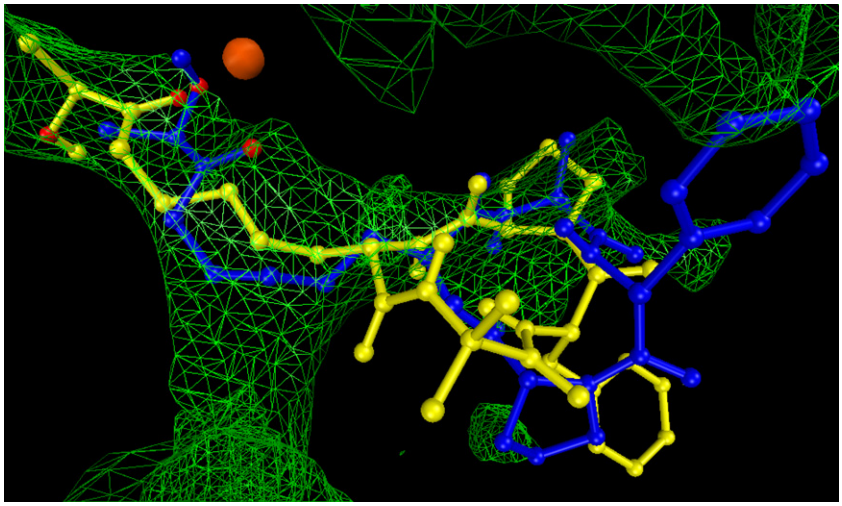

Figure 6. The superimposition of **2** and **6** in the zinc-binding site. The green mesh represents the hydrophobic pocket of the protein. The Zn^{2+} is represented by a CPK sphere in dark orange. Compound **2** is shown by sticks and balls (dark blue); Compound **6** is depicted by sticks and balls (yellow). The figure highlights the similar interactions with the 11 Å deep hydrophobic channel of the Ahoda side chains, whereas the α-hydroxyl ketone groups of **2** and **6** coordinate the zinc ion in different fashion.

For compounds **6**–**10**, presenting an inverted absolute configuration of C9 compared to FR235222 and **1**–**5**, the docking results revealed that both isomers show different possible binding modes (as observed for **5**). These docked conformations do not efficiently interact with all the structural portions, giving unstable complex with the target. Moreover, in most cases we obtained good calculated K_i comparable with **2**–**4**, but the Ahoda side chain did not interact with the 11 Å deep hydrophobic channel. In particular we observed, for **6**–**10**, that the zinc ion was coordinated only by one oxygen, but the second heteroatom was not involved in hydrogen bonds pointing far away from amino acids of catalytic site. In Figure 6, the superimposition of the two diasteroisomers **2** and **6**, only differing for the absolute configuration of C9 is shown. The comparison of **2** and **6** in the catalytic site shows that the configuration of C9 is determining for the different spatial arrangements of the oxygen atoms approaching the zinc ion.

The α-hydroxyl ketone group, losing essential interactions with the amino acids involved in the catalytic mechanism, let predict a lower binding affinity as confirmed by biological assays (Table 1).[6] The compounds **6**–**10** indeed presented higher IC_{50} values than **1**–**5**, even if **6** and **7** still inhibited the enzyme activity in nanomolar range.

4. Conclusions

The natural cyclopeptide FR235222 has been used as lead compound for the generation of new and more effective antitumor therapeutics, because it showed a potent inhibition activity on HDAC displaying relevant multiple anticancer effects. Recently, we have synthesized a small collection of FR235222 simplified analogues which presented interesting biological activities, in particular **1**–**3** had a better inhibition properties compared to the natural progenitor. These results encouraged us to further explore the structural determinants responsible for the activity of this class of HDAC inhibitors in order to gain guidelines for the rational design of new derivatives with putative higher affinity for this target. The structural investigations of the new compounds were performed by solution structure determinations, through 2D NMR spectroscopy, followed by docking studies.

The NMR spectra of all cyclotetrapeptides showed a double pattern of resonances due to *cis*–*trans* conformational equilibrium of peptide bond formed by amine and carboxylic groups of proline and phenylalanine residues respectively. Thus, the solution structures of *cis*- and *trans*-*isomers* for **1**–**10** were elucidated and then their energies and geometries were optimized at DFT level and used as starting conformations in docking calculations. The out-

comes of docking studies have revealed that structure **1**, in *cis* and *trans* conformation, presented the best affinity for the target. The analysis of docked conformations indicated that hydrophobic interactions contributed mostly to the stability of the complex. In particular, the indole ring, structural portion of **1**, was able to interact efficiently with hydrophobic pockets located at the rim of zinc-containing tubular cavity. Moreover, we found for **1**–**4** that both isomers formed a stable complex with HDLP, whereas structure **5** presented only one isomer with a defined bioactive conformation with a calculated binding affinity comparable with the values obtained for **2**–**4**. These docking data suggested that both effective interactions with protein and the double contribution of two isomers to bind the biological target affected the HDAC inhibition as was confirmed by biological essays.

In agreement with experimental results, the analysis of **6**–**10** docked poses revealed different possible bioactive conformations, predicting the formation of weak complexes with HDLP. Moreover, the analogues **6**–**10** were designed and synthesized with an inverted absolute configuration to C9 respect to FR235222 and **1**–**5**, to evaluate the influence on the α-hydroxy-ketone zinc-chelating function. Docking data indicated that analogues **6**–**10** coordinated the zinc ion by only one of two oxygen of α-hydroxy-ketone group and lost hydrogen bonds formed by the second oxygen with amino acids of catalytic site.

The change in C9 configuration causes a lowering in the binding affinities but does not lead to a complete loss of HDAC inhibition activities, in particular for compounds **6** and **7**. On the basis of this theoretical results we cannot assess the interfering role of C9 configuration with the enzymatic activity, so further studies are necessary. A future step is to synthesize diastereoisomers of our small collection of compounds (**1**–**10**), differing from preceding analogues for the C9 configuration.

The collected data on structure–activity relationship suggest to insert in the primary sequence more than one amino acid with bulky hydrophobic side chains, like two tryptophan units. Such units can provide both hydrophobic interactions and significant hydrogen bonds. We also advise, to allow better interaction with hydrophobic cavities on protein surface, to alternate amino acids with bulky hydrophobic side chains in the primary sequence, as highlighted by superimposition of both isomers of **1** in the active site.

Our docking studies have been performed using, for the binding energy calculation, protein parameters previously optimized in a recent analysis on other bioactive tetrapeptide ligands, reaching a good qualitative accordance between theoretical K_D and biological essays results. In particular, we calculated the partial charges of HDLP catalytic center (formed by Zn and amino acids A169, H170, D168, and D258) at quantum mechanical level and used for van der Waals term the well depth and zinc radius proposed by Stote et al. In the present contribution, we also obtained a calculated affinities trend comparable with experimental one, validating our target model.

5. Experimental methods

5.1. NMR experiments

All NMR experiments (^{1}H, ^{1}H–^{13}C HSQC[14], ^{1}H–^{13}C HMBC, TOCSY[15], COSY, ROESY[16]) were recorded on a Bruker DRX600 spectrometer, fitted with cryoprobe, at $T = 300$ K. All spectra were acquired in the phase-sensitive mode, and the TPPI method[17] was used for quadrature detection in the ω_1 dimension. For the 2D spectra, the compounds were dissolved in 0.2 mL of DMSO-d_6 99.95%. The spectra were calibrated using the solvent signal as internal standard (^{1}H, $\delta = 2.50$ ppm; ^{13}C, $\delta = 39.5$ ppm).

The ROESY[16] spectra were executed with a mixing time of 100 ms.

The NMR data were processed on a Silicon Graphic Indigo2 workstation using UXNMR software.

5.2. Molecular mechanics and dynamics calculations

Molecular mechanics/dynamics (MM and MD) calculations were performed on a Pentium IV 2800 MHz using the Macromodel 8.5 software[18] package and the MMFFs force field.[19] Monte-Carlo multiple minimum (MCMM) method (50,000 steps) was first used in order to allow a full exploration of the conformational space. Subsequently, in order to refine the so-obtained structures, molecular mechanics and dynamics were performed using a set of distance restraints obtained by the ROESY data (100 ms mixing time). The ROEs intensities were pooled in strong, medium, and weak, setting the upper bound to 2.7 Å for strong ROEs, 3.3 Å for medium ROEs, and 5.0 Å for weak ROEs.[20]

Once the ROEs intensities were collected (as described above), to obtain a better distance restraints distribution, a distance calibration (r^{-6}, two-spin approximation) was used to convert the most intense and significant ROESY cross peak volumes in the distance restraints. A penalty of 50 kJ/Å^2 was applied for the distance violations. A temperature of 500 K was used during the dynamics simulations and a standard constant temperature velocity-Verlet algorithm was used to integrate the equations of motions. A constant dielectric term ($\varepsilon = 48$), mimicking the presence of DMSO, was used in the calculations for reducing the artifacts derived from the absence of the solvent. For structures **8** and **9**, molecular mechanics and dynamics were performed without a set of distance restraints at a temperature of 500 K. All the structures were minimized using a Polak-Ribiere Conjugate Gradient (PRCG, 50,00,000 steps, convergence threshold 0.005 kJ mol^{-1} Å^{-1}).

5.3. Docking studies

Autodock 3.0.5[11] was used for all docking calculations. HDLP (histone deacetylase-like protein) is a metalloprotein, so a nonbonded model for metallic center according to the nonbonded Zn parameters of Stote and Karplus[9] (zinc radius = 1.10 Å, well depth = 0.25 kcal/mol) was used. In order to have an accurate weight of the electrostatics, we used the previously derived partial charge of Zn = 1.175 and of the amino acids involved in the catalytic center (A169, H170, D168, D258) by DFT as described in our previous work.[7] As for what concerns the ligands, the NMR-derived geometries were optimized at the hybrid DFT B3LYP level using the 6-31G(d) basis set (Gaussian 03 Software Package).[21] Subsequently, the charges of **1**–**10** *cis*- and *trans*-structures were calculated with the ChelpG method[13] at the B3LYP/6-31G+(d) level. The above calculated charges were used for docking calculations. For all the docking calculations, a grid box size of $66 \times 64 \times 64$ with spacing of 0.375 Å between the grid points, centered between Zn^{2+} and H170, and covering the catalytic center surface of HDLP was used. For all the docked structures, all bonds were treated as active torsional bonds except the amide bonds. In order to achieve a representative conformational space during the docking calculations, six calculations consisting of 256 runs were performed, obtaining 1536 structures (256×6). The Lamarkian genetic algorithm was used for dockings. An initial population of 150 randomly placed individuals, a maximum number of 2.5×10^5 energy evaluations, and a maximum number of 2.7×10^4 generations were taken into account. A mutation rate of 0.02 and a crossover rate of 0.8 were used. Results differing by less than 2 Å in positional root-mean-square deviation (RMSD) were clustered together and represented by the result with the most favorable free energy of binding.

The selection criteria of bioactive conformation was the evaluation of statistical relevance of clusters and the free energy of binding. Moreover, the interactions with 11 Å hydrophobic channel and the zinc ion were taken into account.

Supplementary data

Supplementary data associated with this article can be found, in the online version, at doi:10.1016/j.bmc.2008.08.003.

References and notes

1. Biel, M.; Wascholowski, V.; Giannis, A. *Angew. Chem., Int. Ed.* **2005**, *44*, 3186.
2. Momparler, R. L. *Oncogene* **2003**, *22*, 6479.
3. (a) Bolden, J. E.; Peart, M. J.; Johnstone, R. W. *Nat. Rev.* **2006**, *5*, 769; (b) Lin, H.-Y.; Chen, C.-S.; Lin, S.-P.; Weng, J.-R.; Chen, C.-S. *Med. Res. Rev.* **2006**, *26*, 397; (c) Xu, W. S.; Parmigiani, R. B.; Marks, P. A. *Oncogene* **2007**, *26*, 5541.
4. (a) Mori, H.; Urano, Y.; Kinoshita, T.; Yoshimura, S.; Takase, S.; Hino, M. *J. Antibiot.* **2003**, *56*, 181; (b) Mori, H.; Abe, F.; Furukawa, S.; Sakai, F.; Hino, M.; Fujii, T. *J. Antibiot.* **2003**, *56*, 80–86; (c) Mori, H.; Urano, Y.; Abe, F.; Furukawa, S.; Tsurumi, Y.; Sakamoto, K.; Hashimoto, M.; Takase, S.; Hino, M.; Fujii, T. *J. Antibiot.* **2003**, *56*, 72–79.
5. (a) Rodriquez, M.; Terracciano, S.; Cini, E.; Settembrini, G.; Bruno, I.; Bifulco, G.; Taddei, M.; Gomez-Paloma, L. *Angew. Chem., Int. Ed.* **2006**, *45*, 423; (b) Xie, W.; Zou, B.; Pei, D.; Ma, D. *Org. Lett.* **2005**, *7*, 2775; (c) Petrella, A.; D'Acunto, C. W.; Rodriquez, M.; Festa, M.; Tosco, A.; Bruno, I.; Terracciano, S.; Taddei, M.; Gomez Paloma, L.; Parente, L. *EJC* **2008**, *44*, 740.
6. Gomez-Paloma, L.; Bruno, I.; Cini, E.; Khochbin, S.; Rodriquez, M.; Taddei, M.; Terracciano, S.; Sadoul, K. *ChemMedChem* **2007**, *2*, 1511.
7. Maulucci, N.; Chini, M. G.; Di Micco, S.; Izzo, I.; Cafaro, E.; Russo, A.; Gallinari, P.; Paolini, C.; Nardi, M. C.; Casapullo, A.; Riccio, R.; Bifulco, G.; De Riccardis, F. J. *Am. Chem. Soc.* **2007**, *129*, 3007.
8. (a) Finnin, M. S.; Donigian, J. R.; Cohen, A.; Richon, V. M.; Rifkind, R. A.; Marks, P. A.; Breslow, R.; Pavletich, N. P. *Nature* **1999**, *401*, 188; (b) Vannini, A.; Volpari, C.; Filocamo, G.; Casavola, E. C.; Brunetti, M.; Renzoni, D.; Chakravarty, P.; Paolini, C.; De Francesco, R.; Gallinari, P.; Steinkühler, C.; Di Marco, S. *Proc. Natl. Acad. Sci. U.S.A.* **2004**, *101*, 15064; (c) Wang, D.-F.; Wiest, O.; Helquist, P.; Lan-Hargest, H.-Y.; Wiech, N. L. J. *Med. Chem.* **2004**, *47*, 3409.
9. Stote, R. H.; Karplus, M. *Proteins* **1995**, *23*, 12.
10. (a) Chazin, W. J.; Kordel, J.; Drakenberg, T.; Thulin, E.; Brodin, P.; Grundstrom, T.; Forsen, S. *Proc. Natl. Acad. Sci. U.S.A.* **1989**, *86*, 2195–2198; (b) Sikorska, E.; lusarz, R. S.; Lammek, B. J. *Peptide Res.* **2005**, *66*, 30.
11. Morris, G. M.; Goodsell, D. S.; Halliday, R. S.; Huey, R.; Hart, W. E.; Belew, R. K.; Olson, A. J. J. *Comp. Chem.* **1998**, *19*, 1639.
12. (a) Wang, D.-F.; Helquist, P.; Wiech, N. L.; Wiest, O. J. *Med. Chem.* **2005**, *48*, 6936; (b) Park, H.; Lee, S. J. *Comput.-Aided Mol. Des.* **2004**, *18*, 375.
13. Breneman, C. M.; Wiberg, K. B. J. *Comp. Chem.* **1990**, *11*, 361.
14. (a) Palmer, A. G.; Cavanagh, J.; Wright, P. E.; Rance, M. J. *Magn. Reson.* **1991**, *93*, 151; (b) Kay, L. E.; Keifer, P.; Saarinen, I. J. *Am. Chem. Soc.* **1992**, *114*, 10663; (c) Schleucher, J.; Schwendinger, M.; Sattler, M.; Schimdt, P.; Sched, O.; Glaser, S. J.; Sorensen, O. W.; Griesinger, C. J. *Biomol. NMR* **1994**, *4*, 301; (d) Willker, W.; Leibfritz, D.; Kerssebaum, R.; Bermel, W. *Magn. Reson. Chem.* **1993**, *31*, 287.
15. Bax, A.; Davis, D. G. *J. Magn. Reson.* **1985**, *65*, 355.
16. Bax, A.; Davis, D. G. *J. Magn. Reson.* **1985**, *63*, 207.
17. Marion, D.; Wüthrich, K. *Biochem. Biophys. Res. Commun.* **1983**, *113*, 967.
18. MacroModel, version 8.5, Schrödinger LLC, New York, NY, 2003.
19. Mohamadi, F.; Richards, N. G.; Guida, W. C.; Liskamp, R.; Lipton, M.; Caufield, C.; Chang, G.; Hendrickson, T.; Still, W. C. *J. Comput. Chem.* **1990**, *11*, 440.
20. Williamson, M. P.; Havel, T. F.; Wüthrich, K. *J. Mol. Biol.* **1985**, *182*, 295.
21. Frisch, M. J.; Trucks, G. W.; Schlegel, H. B.; Scuseria, G. E.; Robb, M. A.; Cheeseman, J. R.; Montgomery, J. A., Jr.; Vreven, T.; Kudin, K. N.; Burant, J. C.; Millam, J. M.; Iyengar, S. S.; Tomasi, J.; Barone, V.; Mennucci, B.; Cossi, M.; Scalmani, G.; Rega, N.; Petersson, G. A.; Nakatsuji, H.; Hada, M.; Ehara, M.; Toyota, K.; Fukuda, R.; Hasegawa, J.; Ishida, M.; Nakajima, T.; Honda, Y.; Kitao, O.; Nakai, H.; Klene, M.; Li, X.; Knox, J. E.; Hratchian, H. P.; Cross, J. B.; Adamo, C.; Jaramillo, J.; Gomperts, R.; Stratmann, R. E.; Yazyev, O.; Austin, A. J.; Cammi, R.; Pomelli, C.; Ochterski, J. W.; Ayala, P. Y.; Morokuma, K.; Voth, G. A.; Salvador, P.; Dannenberg, J. J.; Zakrzewski, V. G.; Dapprich, S.; Daniels, A. D.; Strain, M. C.; Farkas, O.; Malick, D. K.; Rabuck, A. D.; Raghavachari, K.; Foresman, J. B.; Ortiz, J. V.; Cui, Q.; Baboul, A. G.; Clifford, S.; Cioslowski, J.; Stefanov, B. B.; Liu, G.; Liashenko, A.; Piskorz, P.; Komaromi, I.; Martin, R. L.; Fox, D. J.; Keith, T.; Al-Laham, M. A.; Peng, C. Y.; Nan, ayakkara, A.; Challacombe, M.; Gill, P. M. W.; Johnson, B.; Chen, W.; Wong, M. W.; Gonzalez, C.; Pople, J. A. Gaussian 03, revision B.05; Gaussian: Pittsburgh, PA, 2003.